Variance-constrained control of maneuvering helicopters with sensor failure

Tugrul Oktay and Cornel Sultan

Proceedings of the Institution of Mechanical Engineers, Part G: Journal of Aerospace Engineering published online 23 October 2012
DOI: 10.1177/0954410012464002

Original Article

Institution of MECHANICAL ENGINEERS
Journal of AEROSPACE ENGINEERING

Proc IMechE Part G:
J Aerospace Engineering
0(0) 1–14

DOI: 10.1177/0954410012464002
uk.sagepub.com/jaero
SAGE

Variance-constrained control of maneuvering helicopters with sensor failure

Tugrul Oktay and Cornel Sultan

Abstract

This article presents the novel results obtained using variance-constrained controllers and maneuvering helicopters also when some helicopter sensors fail. For this purpose, complex, control oriented, and physics-based helicopter models are used. A nonlinear model of the helicopter, which includes blade flexibility, is first linearized around specific maneuvering flight conditions (i.e. level banked turn and helical turn). The resulting linearized models are used for the design of variance-constrained controllers (i.e. output and input variance-constrained controllers). Then, the robustness of the closed-loop systems with respect to modeling uncertainties (i.e. flight conditions and helicopter inertial parameters variations) is studied. Next, variance-constrained controllers are designed for these maneuvering helicopter models when some helicopter sensors fail. Several sensor failure cases are examined and robustness properties of the closed-loop systems with respect to modeling uncertainties are also examined. Limitations of the control design process due to the number and type of failed sensors are investigated as well. Finally, the possibility to adaptively switch between controllers in order to mitigate sensor failure is studied.

Keywords

Maneuvering flight, variance-constrained controllers, robustness, adaptive switching

Date received: 10 February 2012; accepted: 17 September 2012

Introduction

For maneuvering flight, control design is critical for safe and performant helicopter operation. In particular, helical turns and banked turns are of major interest. For example, they enable transitioning between two straight level flight conditions and monitoring an area of interest, they also allow armed helicopters to avoid ground attack and possibly engage in air to air combat, etc. In this article, design of modern controllers is analyzed for such maneuvers. Since these maneuvers are highly constrained, any control design should account for constraints on outputs and inputs. Therefore, in this article, variance-constrained controllers with inequality constraints on outputs or inputs are analyzed.

Historically, helicopter flight control system design techniques evolved from pole assignment methods[1–3] (which were used since the early days of helicopter flight and control) to simple feedback control approaches,[4–6] followed by modern control methods based on linear matrix algebra like linear quadratic regulator (LQR) and linear quadratic Gaussian (LQG) approaches[7–10] (introduced in the 1970s), as well as H_∞ control synthesis[11–13] (introduced in the 1980s). This evolution was prompted by the difficulties faced by the control designer. For example, classical control methods, which historically came first, are adequate for single-input–single-output systems, but helicopters are strongly coupled multi-input–multi-output (MIMO) systems and control design should simultaneously address requirements for all the dynamic modes of interest. Addressing this multi-variable/multi-objective control problem became possible only with the advent of modern control theory. In this context, linear quadratic control theory has received great attention due to its many advantages. For example, it provides simple solutions via Riccati equations, it is easy to implement, and the relation between the

Department of Aerospace and Ocean Engineering, Virginia Polytechnic Institute and State University, USA

Corresponding author:
Tugrul Oktay, Faculty of Aeronautics and Astronautics, Erciyes University, Kayseri, 38039, Turkey; previously with Virginia Polytechnic Institute and State University.
Email: tugruloktay52@gmail.com

optimal control and state variables is linear. However, weighting matrices for classical LQR and LQG approaches are generally selected ad hoc and the LQG approach does not have guaranteed stability robustness properties. The need for robust design actually prompted the control designer to use H_∞ in helicopter control. For H_∞, control robustness is indeed guaranteed, but it comes at the price of having to design an over-conservative controller, thus usually compromising the optimality of other performance indices (e.g. control energy). A very recent direction in helicopter control, due to the its ability to handle multiple constraints, is model predictive control, in general in connection with models identified using neural networks.[14–16] Nonlinear control theory is also employed recently in helicopter control system design,[14–16] but the control designer faces major difficulties due to implementation, certification, computational complexity, and robustness issues.

The development of the models used for control design in this article is presented in detail in Oktay[17] (see also Oktay and Sultan[18,19]). The main philosophy of the modeling process is to develop physics-based control oriented models that capture the 'essential dynamics'. Essential dynamics does not represent only the dynamics directly controlled (e.g. flight dynamics modes) but also dynamics that is directly affected by control design and which is crucial for safe and performant operation (e.g. flapping, lead–lagging, and blade flexibility).

The modern controllers we employ in this article are variance-constrained controllers. They present several benefits.[20–28] First, these controllers are enhanced-LQG controllers which use state estimators (i.e. Kalman filters). State estimators are crucial for complex systems such as maneuvering helicopters, because some states cannot be easily measured. Second, these controllers use second-order information, specifically the state covariance matrix. This is very important for multi-variable control design because all stabilizing controllers are parameterized in terms of the state covariance matrix, which is physically meaningful. Third, for strongly coupled, large MIMO systems, like the ones encountered in helicopter control and particularly in our work,[17] variance-constrained control design methods provide guarantees on the transient behavior of individual variables by enforcing upper bounds on the variance of these variables.

Because the dynamics of the helicopter is subject to stringent output and input limitations, the performance of variance-constrained controllers is investigated. These controllers are specifically designed to satisfy bounds on output or input variances.[20–27] Such controllers are designed for linearized models and several maneuvering flight conditions, monitoring: (a) speed of convergence of solution algorithms; (b) stability of the closed-loop (CL) systems; and (c) satisfaction of constraints. Moreover, because all systems are subject to modeling uncertainties, CL stability robustness is comprehensively evaluated by varying helicopter's speed and inertial properties. Preliminary studies on variance-constrained controllers for helicopter models were presented in Oktay and Sultan,[22] but without sensor failure analysis and using very simple examples. Variance-constrained controllers were also used in other aerospace applications (e.g. Hubble space telescope, see Skelton and Lorenzo[23]).

An important issue in helicopter control is management of sensor failure. Physical (direct) redundancy, which means adding duplicate or even multiple sensors, is sometimes used for aerospace vehicles. This approach has many limitations.[29,30] For example, some sensors can be very expensive, and there are stringent space limitations on board helicopters which limit the number of sensors that can be carried. Moreover, placement of specific sensors is predetermined due to physical and operational conditions. For example, if all sensors measuring the same quantity are placed in a certain region of the helicopter, a physical phenomenon (e.g. regional stall, flow separation, etc.) may cause failure of these sensors all together. Therefore, different approaches, in which mathematical relations are used to obtain redundant measurements, are being developed recently.[30–34]

In this article, an alternative approach, namely adaptive switching between controllers which are adequate for different sets of sensors, but provide the same prespecified performance, is proposed. This approach has nowadays become possible due to recent advances in control theory, signals processing, microelectronics, power electronics, and microprocessors. Switching between controllers can then be easily and reliably implemented electronically, thus not requiring addition of mass. The idea investigated is if one can adaptively change the controller in flight to satisfy the same constraints when the set of measurements changes due to sensor failure. Therefore, variance-constrained controllers are also studied with different sets of measurements.

Mathematical model

The helicopter model used in this study includes fuselage, tail rotor, landing gear, horizontal tailplane, fully articulated main rotor (i.e. with four blades), and main rotor downwash.[17] Linear aerodynamics is assumed for each helicopter component and blade flexibility is considered. The mathematical model of the maneuvering helicopter has 9 fuselage equations, 16 blade flapping and lead–lagging equations, 16 blade flexibility equations, 3 static main rotor downwash equations, and 1 algebraic flight path angle equation (see Oktay[17] for details). These governing equations of motion in implicit form are

$$\boldsymbol{f}(\dot{\boldsymbol{x}}, \boldsymbol{x}, \mathbf{u}) = 0 \tag{1}$$

where $\boldsymbol{f} \in \mathbb{R}^{45}$, $x \in \mathbb{R}^{41}$($\boldsymbol{x}$ is the nonlinear state vector), and $\boldsymbol{\upsilon} \in \mathbb{R}^4$ ($\boldsymbol{\upsilon}$ is the nonlinear control vector).

Maneuvers

In this study, level banked turn without sideslip and helical turn without sideslip are examined.[35–39] For maneuvering flight, the aircraft linear velocities are (Figure 1)

$$\begin{bmatrix} u & v & w \end{bmatrix}^T = \begin{bmatrix} V_A\cos(\alpha_F)\cos(\beta_F) & V_A\sin(\beta_F) & V_A\sin(\alpha_F)\cos(\beta_F) \end{bmatrix}^T \quad (2)$$

where fuselage angle of attack, α_F, and sideslip, β_F, are given by

$$\alpha_F = \tan^{-1}(w/u), \quad \beta_F = \sin^{-1}(v/V_A) \quad (3)$$

Level banked turn is a maneuver in which the helicopter banks towards the center of the turning circle. For helicopters, the fuselage roll angle, ϕ_A, is in general slightly different than the bank angle, ϕ_B. For coordinated banked turn $\phi_A = \phi_B$. A picture describing these angles for a particular case ($\theta_A = 0$) is given in Figure 2, where $F_{\text{resultant}}$ is the sum of the gravitational force (W) and the centrifugal force (F_{cf}).

Helical turn is a maneuver in which the helicopter moves along a helix with constant speed (Figure 3). In a helical turn, the flight path angle is different than zero being given by

$$\begin{aligned} \sin(\gamma_{FP}) = {} & \sin(\theta_A)\cos(\alpha_F)\cos(\beta_F) \\ & - \sin(\phi_A)\cos(\theta_A)\sin(\beta_F) \\ & - \cos(\phi_A)\cos(\theta_A)\sin(\alpha_F)\cos(\beta_F) \end{aligned} \quad (4)$$

A picture describing the flight path angle for a particular case, $\phi_A = 0$, $\beta_F = 0$, is given in Figure 4.

Note that $\dot{\psi}_A > 0$ is a clockwise turn and $\dot{\psi}_A < 0$ is a counterclockwise turn (viewed from the top) while $\gamma_{FP} > 0$ is referring to the ascending flight and $\gamma_{FP} < 0$ is referring to the descending flight. Note: the numerical results reported from here on (i.e. for trim, linearization, and control design) were obtained using Puma SA 330 data.[17,40]

Trim and linearization

In this article, trim is defined as the condition for which level banked or helical turn with constant V_A and zero sideslip is achieved. For our helicopter model, 29 trim equations and 29 unknowns were

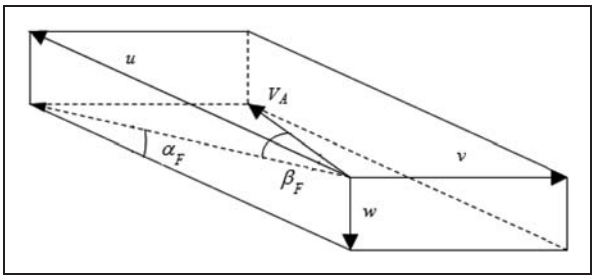

Figure 1. Fuselage angle of attack and sideslip.

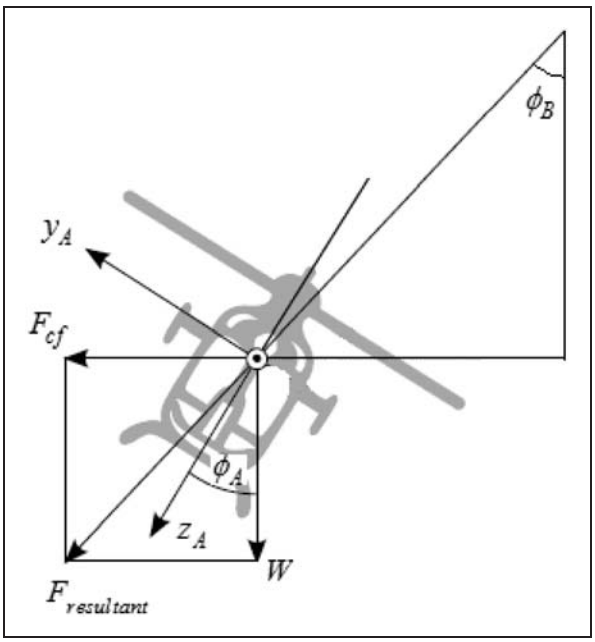

Figure 2. Level banked turn.

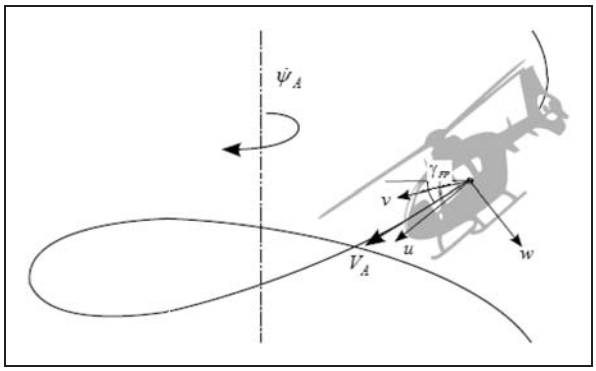

Figure 3. Helical turn.

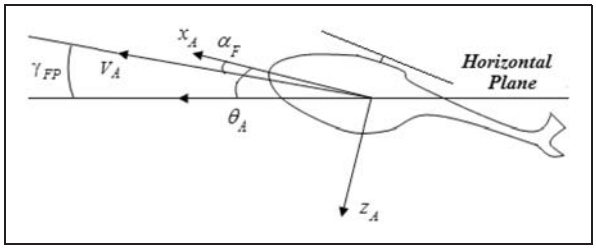

Figure 4. Flight path angle.

obtained (i.e. $0 = 0$ equations are ignored). Matlab *f*solve command was used to solve the 29 trim equations. The results, thus, found were verified by inserting them into the governing equations of motion (equation (1)). Very small numbers (around 10^{-10}) were obtained showing that the trimming procedure is correct. Numerous numerical experiments resulted in trim values that are in the range reported in the literature.[17] After finding trim values, the helicopter model was linearized using Maple, yielding continuous linear time-invariant (LTI) systems

$$\dot{\boldsymbol{x}}_p = \boldsymbol{A}_p \boldsymbol{x}_p + \boldsymbol{B}_p \mathbf{u} \tag{5}$$

where $\boldsymbol{x}_p = \Delta \boldsymbol{x}$ and $\mathbf{u} = \Delta \mathbf{u}$. The resulting modes (flight dynamics modes, flapping, and lead–lagging modes) are very close to the modes reported in Oktay[17] for straight level flight which were validated against available data in the literature.

Variance-constrained controllers

In this article, output variance-constrained control (OVC) and input variance-constrained control (IVC)[20–28] were investigated. The OVC problem is stated next. Given a continuous LTI system

$$\dot{\boldsymbol{x}}_p = \boldsymbol{A}_p \boldsymbol{x}_p + \boldsymbol{B}_p \mathbf{u} + \boldsymbol{D}_p \boldsymbol{w}_p, \boldsymbol{y} = \boldsymbol{C}_p \boldsymbol{x}_p, \boldsymbol{z} = \boldsymbol{M}_p \boldsymbol{x}_p + \boldsymbol{v}_s \tag{6}$$

and a positive definite input penalty $\boldsymbol{R} > 0$, find a full order *dynamic* controller

$$\dot{\boldsymbol{x}}_c = \boldsymbol{A}_c \boldsymbol{x}_c + \boldsymbol{F}\boldsymbol{z}, \mathbf{u} = \boldsymbol{G}\boldsymbol{x}_c \tag{7}$$

to solve the problem

$$\min_{\boldsymbol{A}_c, \boldsymbol{F}, \boldsymbol{G}} E_\infty \mathbf{u}^T \boldsymbol{R} \mathbf{u} \tag{8}$$

subject to

$$E_\infty \boldsymbol{y}_i^2 \leqslant \sigma_i^2, \ i = 1, \ldots, n_y \tag{9}$$

where $\boldsymbol{z}$ represents sensor measurements, $\boldsymbol{w}_p$ and $\boldsymbol{v}_s$ are zero-mean uncorrelated Gaussian white noises with intensities $\boldsymbol{W}$ and $\boldsymbol{V}$, respectively, σ_i^2 the upper bound imposed on the ith output variance, and n_y the number of outputs. OVC solution reduces to a LQG problem solution by choosing output penalty $\boldsymbol{Q} > 0$ depending on the inequality constraints. An algorithm for the selection of $\boldsymbol{Q}$ is presented in Hiseh et al.[24] and Zhu and Skelton.[25] After converging on $\boldsymbol{Q}$, OVC parameters are

$$\begin{aligned} &\boldsymbol{A}_c = \boldsymbol{A}_p + \boldsymbol{B}_p \boldsymbol{G} - \boldsymbol{F}\boldsymbol{M}_p, \boldsymbol{F} = \boldsymbol{X}\boldsymbol{M}_p^T \boldsymbol{V}^{-1} \\ &\boldsymbol{G} = -\boldsymbol{R}^{-1} \boldsymbol{B}_p^T \boldsymbol{K} \end{aligned} \tag{10}$$

where $\boldsymbol{X}$ and $\boldsymbol{K}$ are solutions of two algebraic Riccati equations

$$\begin{aligned} 0 &= \boldsymbol{X}\boldsymbol{A}_p^T + \boldsymbol{A}_p \boldsymbol{X} - \boldsymbol{X}\boldsymbol{M}_p^T \boldsymbol{V}^{-1} \boldsymbol{M}_p \boldsymbol{X} + \boldsymbol{D}_p \boldsymbol{W}_p \boldsymbol{D}_p^T \\ 0 &= \boldsymbol{K}\boldsymbol{A}_p + \boldsymbol{A}_p^T \boldsymbol{K} - \boldsymbol{K}\boldsymbol{B}_p \boldsymbol{R}^{-1} \boldsymbol{B}_p^T \boldsymbol{K} + \boldsymbol{C}_p^T \boldsymbol{Q} \boldsymbol{C}_p \end{aligned} \tag{11}$$

IVC problem is the dual of OVC: for a given output penalty $\boldsymbol{Q} > 0$, a full-order dynamic controller (equation (7)) for equation (6) must be found to solve

$$\min_{\boldsymbol{A}_c, \boldsymbol{F}, \boldsymbol{G}} E_\infty \boldsymbol{y}^T \boldsymbol{Q} \boldsymbol{y} \tag{12}$$

subject to

$$E_\infty \mathbf{u}_i^2 \leqslant \boldsymbol{\mu}_i^2, \ i = 1, \ldots, n_u \tag{13}$$

where $\boldsymbol{\mu}_i^2$ is the upper bound variance imposed on the ith input and n_u the number of inputs. IVC solution reduces to a LQG problem solution by choosing $\boldsymbol{R} > 0$. An algorithm for the selection of $\boldsymbol{R}$ is presented in Zhu and Skelton.[25] After converging on $\boldsymbol{R}$, IVC is obtained using equation (10). Compared to LQG, in OVC and IVC, $\boldsymbol{Q}$ and $\boldsymbol{R}$ are selected such that satisfaction of constraints is guaranteed.

In the following two sections, the sensor measurements are helicopter linear velocities, angular velocities, and Euler angles. Sensor failure is considered in 'Sensor failure' and 'Adaptive switching' sections. The nondimensionalized noise intensities were considered $\boldsymbol{W} = 10^{-7} I_{41}, \boldsymbol{V} = 10^{-7} \boldsymbol{I}_{n_s}$ (n_s is the number of non-failed sensors).

OVC results. OVC performance was evaluated for numerous maneuvering flights (i.e. level banked turn and helical turn with different V_A, $\dot{\psi}_A$, and γ_{FP}). CL stability robustness was also thoroughly investigated. For this purpose, the following scenarios were considered: (a) a controller designed for a nominal flight condition (e.g. $V_A = 40$ kts, $\dot{\psi}_A = 0.1$ rad/s, and $\gamma_{FP} = 0.1$ rad) is used for different V_A (e.g. $V_A = 20$ kts, $\dot{\psi}_A = 0.1$ rad/s, $\gamma_{FP} = 0.1$ rad, etc.), the key question being 'Does this controller stabilize flight conditions that are different from the nominal one?'; (b) a controller designed for an 'inertial certain' model (i.e. when there are *no* variations in helicopter inertial parameters) is used on the same type of model which experiences uncertainties in *all* helicopter inertial parameters (helicopter mass and helicopter inertia matrix elements). The key question is 'Are the corresponding CL systems stable for these significant modeling uncertainties?' Table 1 summarizes some results that answer these questions. Note that in this and next sections sensor failure is not considered. This topic is discussed later.

Description of scenarios studied is given next. The first OVC is designed for the helicopter model which is linearized for $V_A = 40$ kts, $\dot{\psi}_A = 0.1$ rad/s,

$\gamma_{FP} = 0.1$ rad, $R_{\text{turn}} = 204.73$ m and it is evaluated for the same model for different V_A (line 1). The second OVC is designed for the model which is linearized for $V_A = 80$ kts, $\dot{\psi}_A = 0.1$ rad/s, $\gamma_{FP} = 0.1$ rad, $R_{\text{turn}} = 409.46$ m and evaluated for the same model for different V_A (line 2). The third OVC is identical with the first OVC, but it is evaluated for the model with 10% uncertain helicopter inertial parameters for different V_A (line 3). The fourth OVC is identical with the second OVC, but it is evaluated for the model with 10% uncertain helicopter inertial parameters for different V_A (line 4). The design parameters and convergence properties are described next.

OVC design. In all of the numerical experiments reported next the convergence tolerance for the OVC algorithm was 10^{-6}, while $\boldsymbol{\sigma}^2$ was set to $10^{-4}[1 \quad 1 \quad 0.1]$. All OVCs were designed using the helicopter Euler angles as the outputs while the inputs were all four helicopter controls. After four iterations, the OVC design algorithm converges and the first OVC satisfies these constraints with the convergence error 7.2661×10^{-7}. After six iterations, the second OVC satisfies these constraints with the convergence error 2.9103×10^{-7}. In Figure 5, the output and input variances are shown for different V_A for the first OVC. The third and fourth OVCs are identical with the first and second OVCs, respectively, and they are evaluated for the helicopter model with 10% helicopter inertial parameters *reduction* for different V_A. Note that in Figure 6, for $V_A = 40$ kts, the output and input variances are shown for different helicopter inertia variations, respectively. In this figure, $\Delta \boldsymbol{I}/\boldsymbol{I}$ refers to the relative variation in all helicopter inertial properties (all of them are changed by the *same* percentage).

OVC discussion. It can be easily observed from Table 1 that for the helical turn with $\dot{\psi}_A = 0.1$ rad/s and $\gamma_{FP} = 0.1$ rad, the OVCs are robustly stable with respect to (wrt) variations in V_A. The length of stability intervals (L) is also large (first and second lines in Table 1). Note that L can be found using relation $L = [({}_{up}V_A - {}_{low}V_A)/10] + 1$ where ${}_{up}V_A - {}_{low}V_A$ is the velocity range for which stability is achieved. For example, for hover to 80 kts, $L = ((80 - 0)/10) + 1 = 9$. Moreover, OVCs are robustly stable wrt helicopter inertial properties variation (third and

Table 1. Stability robustness analysis for OVC.

	Hover		10 kts		20 kts		30 kts		40 kts		50 kts		60 kts		70 kts		80 kts		
	CL	OL	CL	OL	CL	OL	CL	OL	CL	OL	CL	OL	CL	OL	CL	OL	CL	OL	L
First	ES	U	ES	U	ES	U	ES	U	ES	MS	ES	MS	ES	MS	ES	U	ES	U	9
Second	ES	U	ES	U	ES	U	ES	U	ES	MS	ES	MS	ES	MS	ES	U	ES	U	9
Third	ES	U	ES	U	ES	U	ES	U	ES	MS	ES	MS	ES	MS	ES	U	ES	U	9
Fourth	ES	U	ES	U	ES	U	ES	U	ES	MS	ES	MS	ES	MS	ES	U	ES	U	9

CL: closed loop; OL: open loop; ES: exponentially stable; MS: marginally stable; U: unstable.
L is the number of velocity intervals for which the CL system is ES.

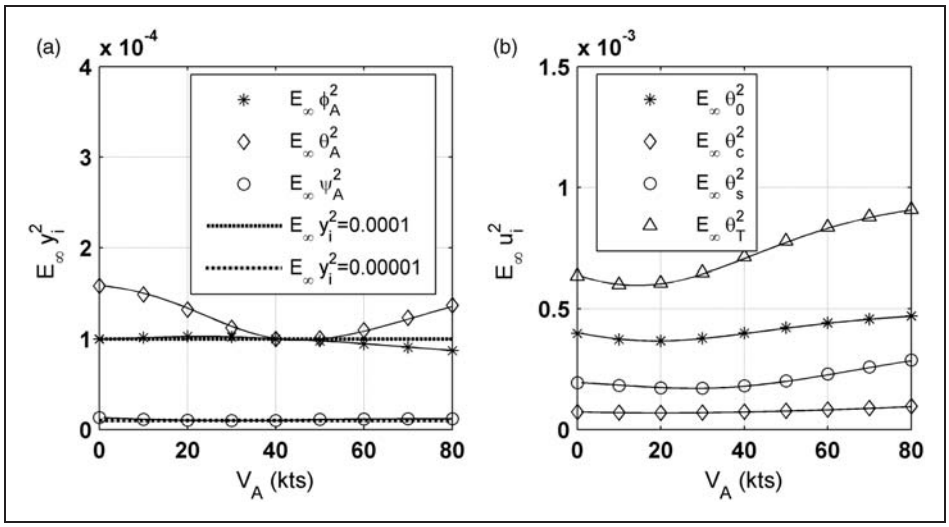

Figure 5. Output and input variances for the first OVC.

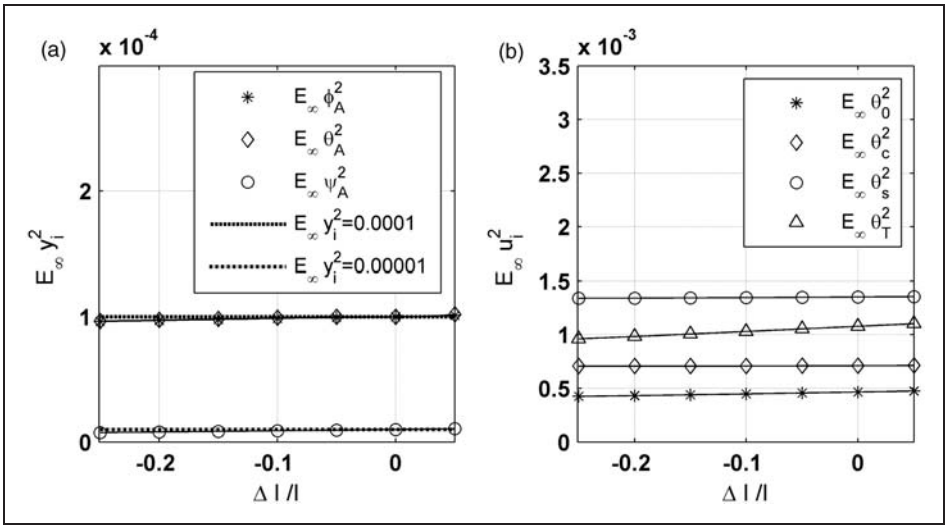

Figure 6. Output and input variances for the Third OVC.

Table 2. Stability robustness analysis for IVC.

	Hover		10 kts		20 kts		30 kts		40 kts		50 kts		60 kts		70 kts		80 kts		
	CL	OL	CL	OL	CL	OL	CL	OL	CL	OL	CL	OL	CL	OL	CL	OL	CL	OL	*L*
First	ES	U	ES	U	ES	U	ES	U	ES	MS	ES	MS	ES	MS	ES	U	ES	U	9
Second	ES	U	ES	U	ES	U	ES	U	ES	MS	ES	MS	ES	MS	ES	U	ES	U	9
Third	ES	U	ES	U	ES	U	ES	U	ES	MS	ES	MS	ES	MS	ES	U	U	U	8
Fourth	ES	U	ES	U	ES	U	ES	U	ES	MS	ES	MS	ES	MS	ES	U	ES	U	9

CL: closed loop; OL: open loop; ES: exponentially stable; MS: marginally stable; U: unstable.

fourth lines in Table 1). Extensive numerical experiments[17] show that OVCs are also robustly stable both wrt variations in V_A and inertial properties for level banked turns and different helical turns. However, it is remarked that L decreases if different values for output constraints are enforced. For example, if for the scenarios described before $\boldsymbol{\sigma}^2$ is *reduced* to $\boldsymbol{\sigma}^2 = 10^{-6}[1 \quad 1 \quad 1]$, L decreases to 4 and 3 for the first and second lines, respectively, in Table 1. Similarly, if $\boldsymbol{\sigma}^2$ is *increased* to $\boldsymbol{\sigma}^2 = 10^{-3}[1 \quad 1 \quad 1]$, L decreases to 5 and 7 for the first and second lines, respectively. These results show that there is no direct correlation between $\boldsymbol{\sigma}^2$ and L (i.e. the dependency between $\boldsymbol{\sigma}^2$ and L is very nonlinear). Figures 5 and 6 indicate that the output variance constraints are satisfied at the nominal flight conditions. If one wants to insure satisfaction of constraints over larger velocity and inertial parameters variation intervals, a safety factor can be introduced in the design. Input variances also display small values.

IVC results

IVCs were evaluated in a similar manner with OVCs. Stability robustness results are summarized in Table 2.

IVC design. In all of the numerical experiments reported next the convergence tolerance for the IVC algorithm was 10^{-7}, while $\boldsymbol{\mu}^2$ was set to $10^{-5}[1 \quad 1 \quad 1 \quad 1]$. All IVCs were designed using *all* four helicopter controls, while the outputs were all three helicopter Euler angles. After 14 iterations, the first IVC satisfies these constraints with the convergence error 6.0214×10^{-8}. After 22 iterations, the second IVC satisfies these constraints with the convergence error 8.3133×10^{-8}. Figure 7 shows the output and input variances for different V_A for the first IVC. The third and fourth IVCs are identical with first and second IVCs, respectively, and they are evaluated for the helicopter model with 10% helicopter inertial quantities *reduction* for different V_A. Note that in Figure 8 for $V_A = 40$ kts, the output and input variances are shown for different helicopter inertia variations, respectively.

IVC discussion. Similarly with the OVCs, IVCs are also robustly stable both wrt variations in V_A and helicopter inertial properties for the helical turn with $\dot{\psi}_A = 0.1$ rad/s and $\gamma_{FP} = 0.1$ rad except that the third IVC does not exponentially stabilize the helicopter when the flight speed is $V_A = 80$ kts. There is no

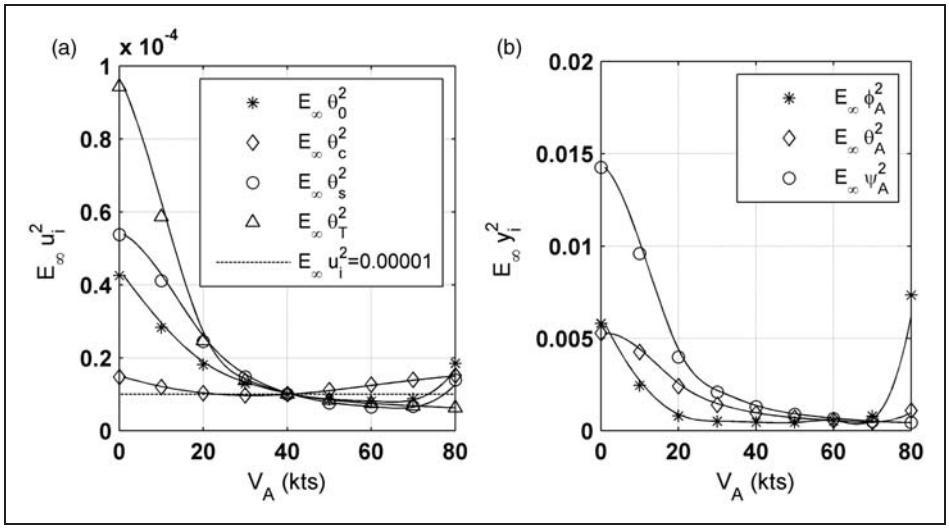

Figure 7. Input and output variances for the first IVC.

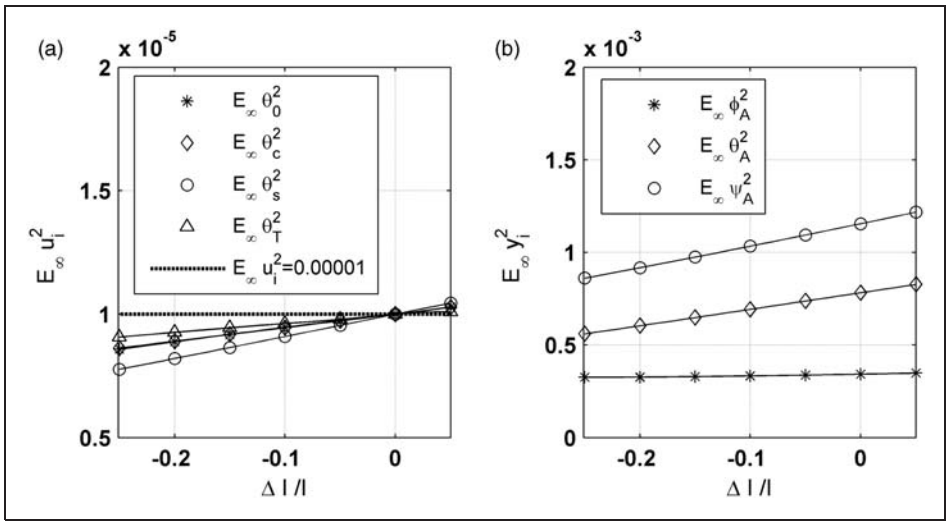

Figure 8. Input and output variances for the third IVC.

direct correlation between the magnitudes of input constraints ($\boldsymbol{\mu}^2$) and length of stability interval (L). Extensive numerical experiments[17] show that IVCs are also robustly stable both wrt variations in V_A and inertial properties for level banked turns and different helical turns. Clearly from Figures 7 and 8, the input variance constraints are satisfied at the nominal flight conditions. Similarly with OVC if one wants to ensure satisfaction of constraints over a larger velocity interval, a safety factor can be introduced in the design. Output variances also display small values.

Sensor failure

Here a new idea, namely adaptive switching between controllers which are adequate for different sets of sensors, but satisfy the same performance requirements, is investigated. The question analyzed next is if the controller can be changed adaptively to satisfy the same variance constraints when the set of measurements changes due to sensor failure. Therefore, in the following sections, OVC and IVC designs are investigated with different sets of measurements.

For this purpose, the same scenarios as in 'OVC results' and 'IVC results' sections were examined. The first to fourth sets of OVCs and IVCs were redesigned using the same models and the same constraints (i.e. $\boldsymbol{\sigma}^2 = 10^{-4}[1 \quad 1 \quad 0.1]$ for OVC, $\boldsymbol{\mu}^2 = 10^{-5}[1 \quad 1 \quad 1 \quad 1]$ for IVC) like for the designs which do not experience sensor failure. The sensor failure scenarios considered are summarized in Tables 3 to 5. The first column in each table displays the measurements that are no longer available due to sensor failure. For example, in the first line of Table 3, ϕ_A

Table 3. CL stability robustness for OVC (CL is ES).

Failed sensors	First	Second	Third	Fourth
First (ϕ_A, θ_A)	Hover to 80 kts	Hover to 80 kts	Hover to 80 kts	Hover to 80 kts
Second (u, v, w)	Hover to 80 kts	Hover to 80 kts	Hover to 80 kts	Hover to 80 kts
Third (p, q, r)	Hover to 80 kts	Hover to 80 kts	Hover to 80 kts	Hover to 80 kts

Table 4. CL stability robustness for IVC (CL is ES).

Failed sensors	First	Second	Third	Fourth
First (ϕ_A, θ_A)	Hover to 80 kts	Hover to 80 kts	Hover to 70 kts	Hover to 80 kts
Second (u, v, w)	20–80 kts	30–80 kts	20–80 kts	30–80 kts
Third (p, q, r)	Hover to 70 kts	Hover to 80 kts	Hover to 70 kts	Hover to 80 kts

Table 5. Control energy comparison.

	OVC cost		IVC cost	
Failed sensors	First and third	Second and fourth	First and third	Second and fourth
First (ϕ_A, θ_A)	0.003607	0.004830	0.001944	0.0006781
Second (u, v, w)	0.001910	0.002633	0.002541	0.0005914
Third (p, q, r)	0.002225	0.0022632	0.001587	0.0004429
No failure	0.001365	0.001526	0.001449	0.0003809

OVC: output variance-constrained control; IVC: input variance-constrained control.

and θ_A measurements from the initial set of nine measurements $(u, v, w, p, q, r, \phi_A, \theta_A, \psi_A)$ are not available thus reducing the set of measurements to seven $(u, v, w, p, q, r, \psi_A)$.

The first important observation is that the number of iterations required to design OVCs and IVCs with sensor failure is usually higher than the number of iterations required when sensor failure does not occur. For example, for the first sensor failure (when ϕ_A and θ_A measurements are not available), the number of iterations for convergence of the first and second OVCs is 18 compared to 4 and 6 iterations when sensor failure does not occur.

It is also observed that the CL stability robustness wrt variations in V_A and helicopter inertial properties are very similar to the ones in 'OVC results' and 'IVC results' sections. The results are summarized in Tables 3 and 4. For example, 'hover to 80 kts' means that the CL system is exponentially stable (ES) for $V_A \in [0, 80]$ kts, $\dot{\psi}_A = 0.1$ rad/s and $\gamma_{FP} = 0.1$ rad. It can be seen from these tables that the length of stability interval (L) for all the sensor failure scenarios is close to L when sensor failure does not occur. The control energy (i.e. cost) of resulting OVCs and IVCs is summarized in Table 5. It can be seen that the control energy of OVCs and IVCs with sensor failure is higher than the control energy when sensor failure does not occur. This is a reflection of the fact that controllers have to work harder to achieve specified variance constraints using less information from sensors. Note that the control energy of OVC and IVC designs was found using[26]

$$J = E_\infty \mathbf{u}^T \boldsymbol{R}\mathbf{u} = \text{trace}\left(\boldsymbol{R}\boldsymbol{G}\boldsymbol{X}_c\boldsymbol{G}^T\right) \tag{14}$$

where $\boldsymbol{G}$ and $\boldsymbol{X}_c$ are computed using OVC and IVC algorithms. For OVC, $\boldsymbol{R}$ is selected by the user, whereas for IVC it is computed using IVC algorithm.

A final important observation is that the results (i.e. number of iterations, stability robustness, input and output variances, and control energy) with sensor failure are qualitatively similar for level banked turns and different helical turns.

We also examined different failure scenarios and limitations of variance-constrained controllers when

Table 6. Large sensor failure scenarios.

Scenario	Active sensors	Failed sensors
Fourth	$(\phi_A, \theta_A, \psi_A)$	(u, v, w, p, q, r)
Fifth	(u, v, w, ψ_A)	$(p, q, r, \phi_A, \theta_A)$
Sixth	(p, q, r, ψ_A)	$(u, v, w, \phi_A, \theta_A)$

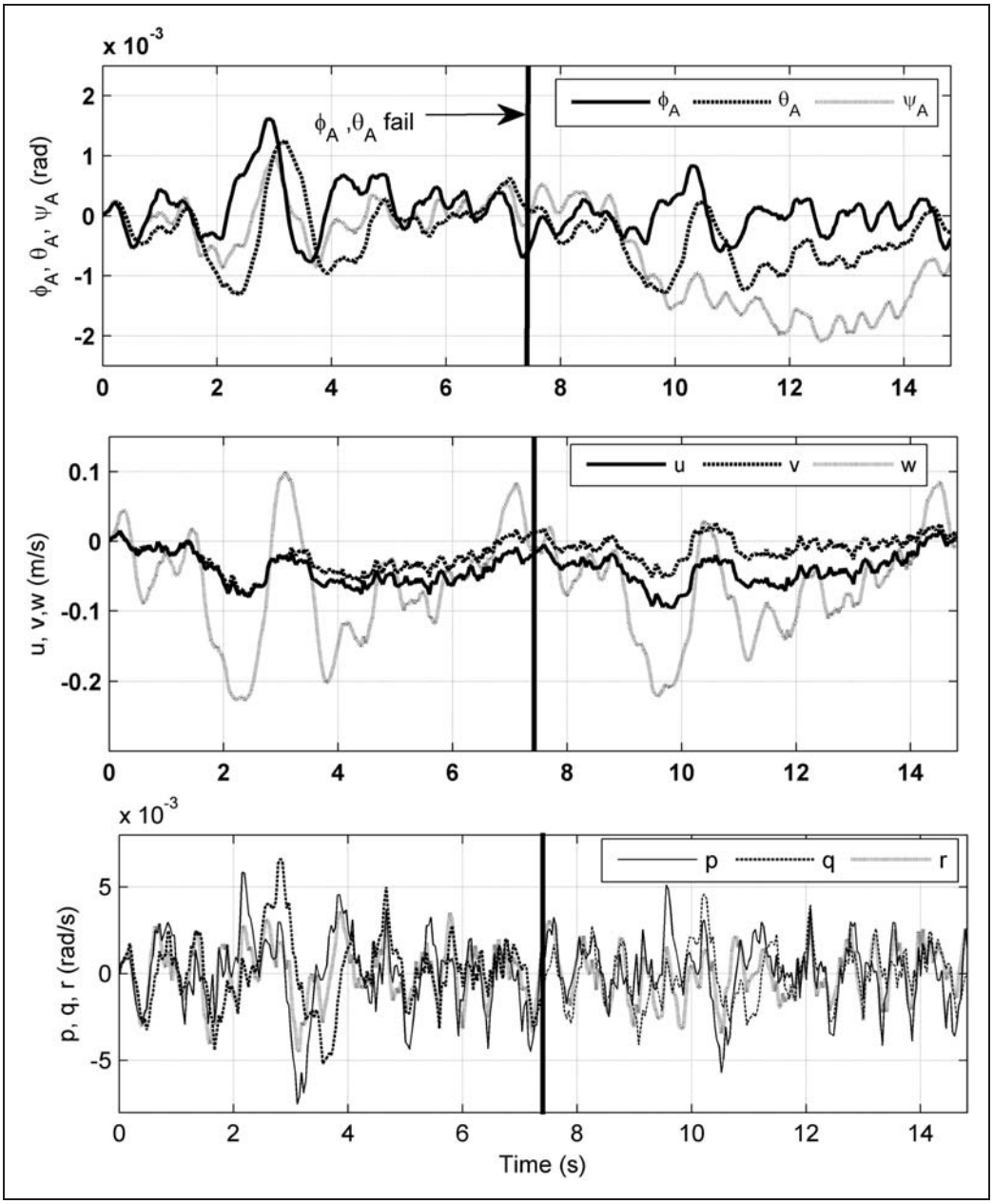

Figure 9. First OVC with first sensor failure (all fuselage states).

large sensor failure occurs. By 'large' in this context we mean that a large number of sensors fail. These additional sensor failure scenarios are summarized in Table 6.

The first key limitation is given by the heading angle (ψ_A) sensor. When this sensor fails variance-constrained controllers cannot be designed and the adaptive switching idea is not feasible due to the fact that the system is not detectable. As LQG-based controllers, variance-constrained controllers require detectability of the system. The best solution for this limitation is to have redundant sensors for the heading angle.

The results (i.e. number of iterations, stability robustness, input and output variances, and control energy) found when the remaining sensors are helicopter Euler angle sensors, i.e. fourth scenario, are very similar with the ones for second or third sensor failure scenarios. On the other hand, when the fifth or sixth scenario occurs, it is not possible to design first to fourth OVCs with constraints $\sigma^2 = 10^{-4}\begin{bmatrix}1 & 1 & 0.1\end{bmatrix}$ or $\sigma^2 = 10^{-6}\begin{bmatrix}1 & 1 & 1\end{bmatrix}$. This reveals a second limitation: prescribed OVC performance cannot be achieved under these failure scenarios. Fortunately, even when the fifth or sixth scenario occurs, it is possible to design OVC by increasing the constraint to $\sigma^2 = 10^{-3}\begin{bmatrix}1 & 1 & 1\end{bmatrix}$. Moreover, it is possible to design first to fourth IVCs with the initial constraint $\mu^2 = 10^{-5}\begin{bmatrix}1 & 1 & 1 & 1\end{bmatrix}$ when fifth or sixth sensor failure occurs.

A third limitation we identified is related to control energy and robustness for IVCs. Specifically,

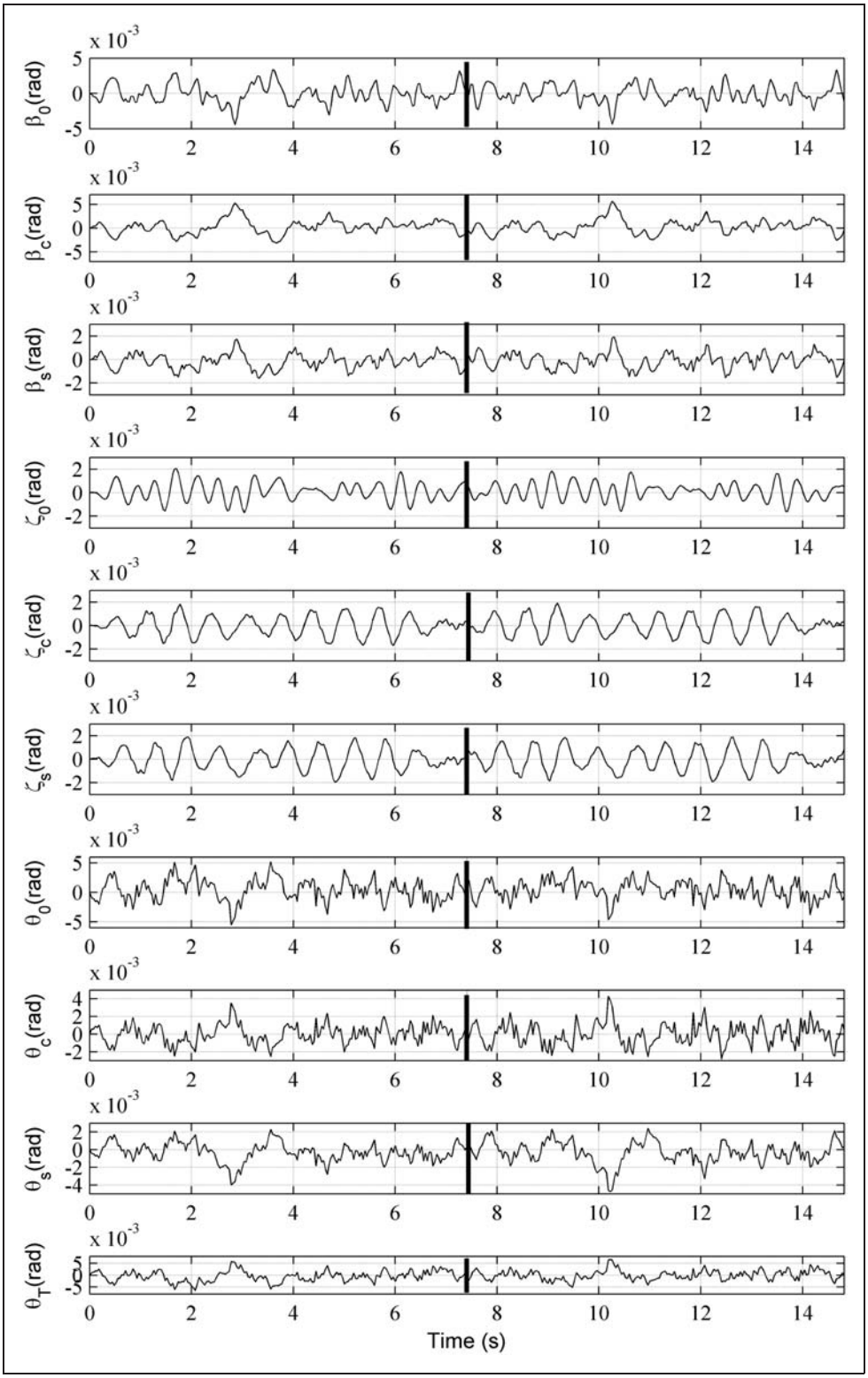

Figure 10. First OVC with first sensor failure (some blade states and all controls).

when the fifth or sixth failure scenario occurs, the results are worse than those obtained when one of the first to third sensor failure scenario occurs. For example, the control energy for the first and third IVCs when the fifth sensor failure scenario occurs is 0.0101 which is much larger than the control energy for the first and third IVCs when one of the first to third failure scenario occurs. Moreover, L is 4 for the second IVC when the fifth sensor failure scenario occurs and this number is less than the Ls for IVCs when one of the first to third failure scenario occurs.

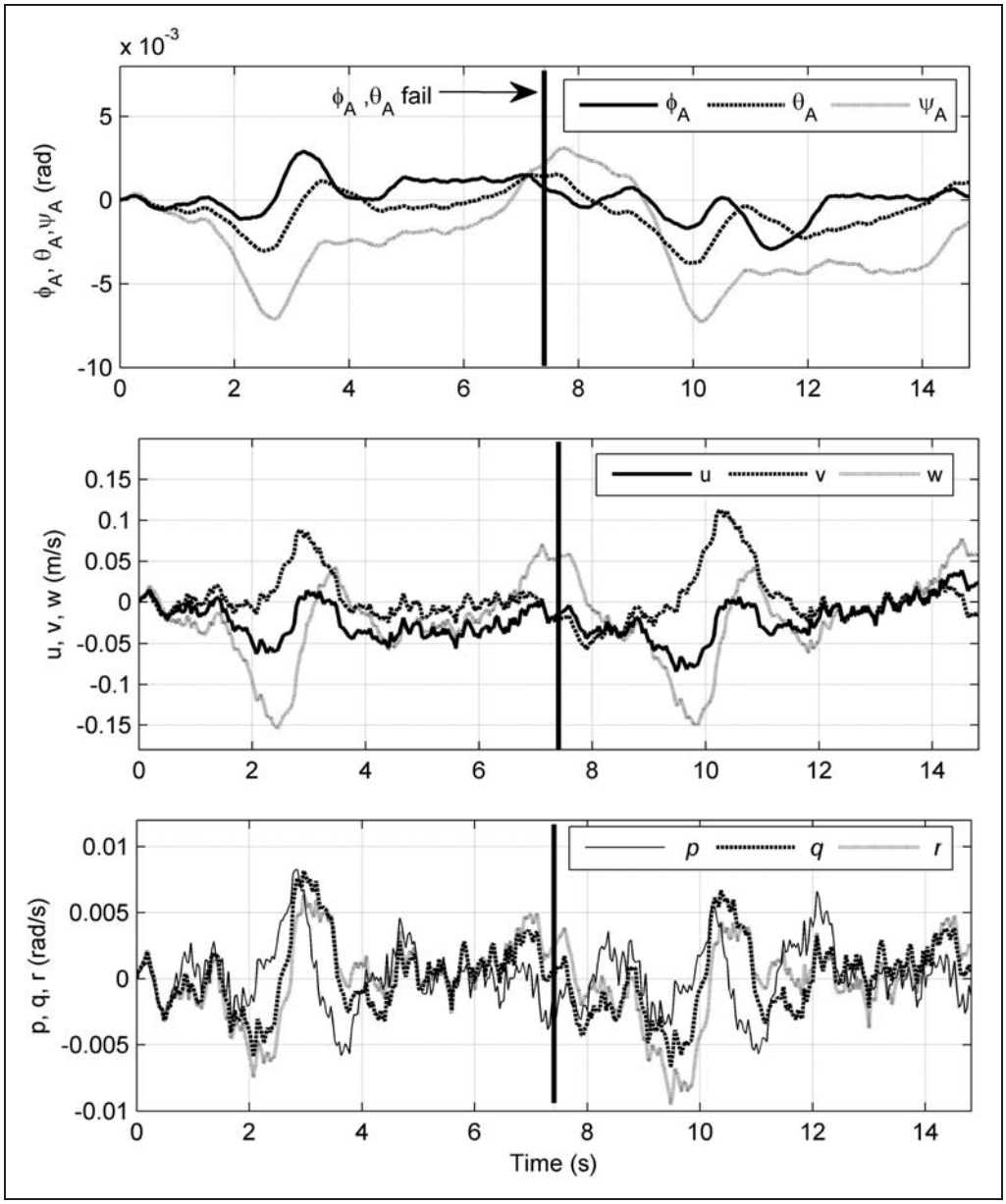

Figure 11. First IVC with first sensor failure (all fuselage states).

Adaptive switching

The behavior of the CL system when switching between controllers occurs due to the first sensor failure scenario for the first OVC and IVC is examined using Matlab. Simulations showed in Figures 9 to 12 indicate that the first OVC and IVC designs are robust to the first sensor failure. In these figures, the bold vertical line represents the instant when ϕ_A, θ_A measurements fail. The sensor failure occurs when $\psi = 200$ rad (or $t = 7.4$ s). The behaviors of all fuselage states and some blade states are shown in Figures 9 to 12. The fuselage states (Figures 9 and 11, plots of u, v, w, p, q, r, ϕ_A, θ_A, and ψ_A) and blade states do not experience large variations (Figures 10 and 12, plots of β_0, β_c, β_s, ζ_0, ζ_c, and ζ_s). Extensive numerical experiments showed that OVC and IVC are robust to other sensor failures (i.e. second and third failures in Tables 3 to 5 and also some large sensor failures). Similar results are found for level banked turns and different helical turns.

Conclusions

Control-oriented, physics-based, and complex helicopter models are used for control design for helical and level banked turns. Models linearized around these flight conditions are used for the design of OVC and IVC. OVC and IVC studies show that all variance-constrained controllers exponentially stabilize the nominal maneuvering flight condition while satisfying the constraints. CL stability robustness analysis reveals that all these controllers are robust when uncertainty in helicopter speed is considered except that the third IVC does not exponentially stabilize when the flight

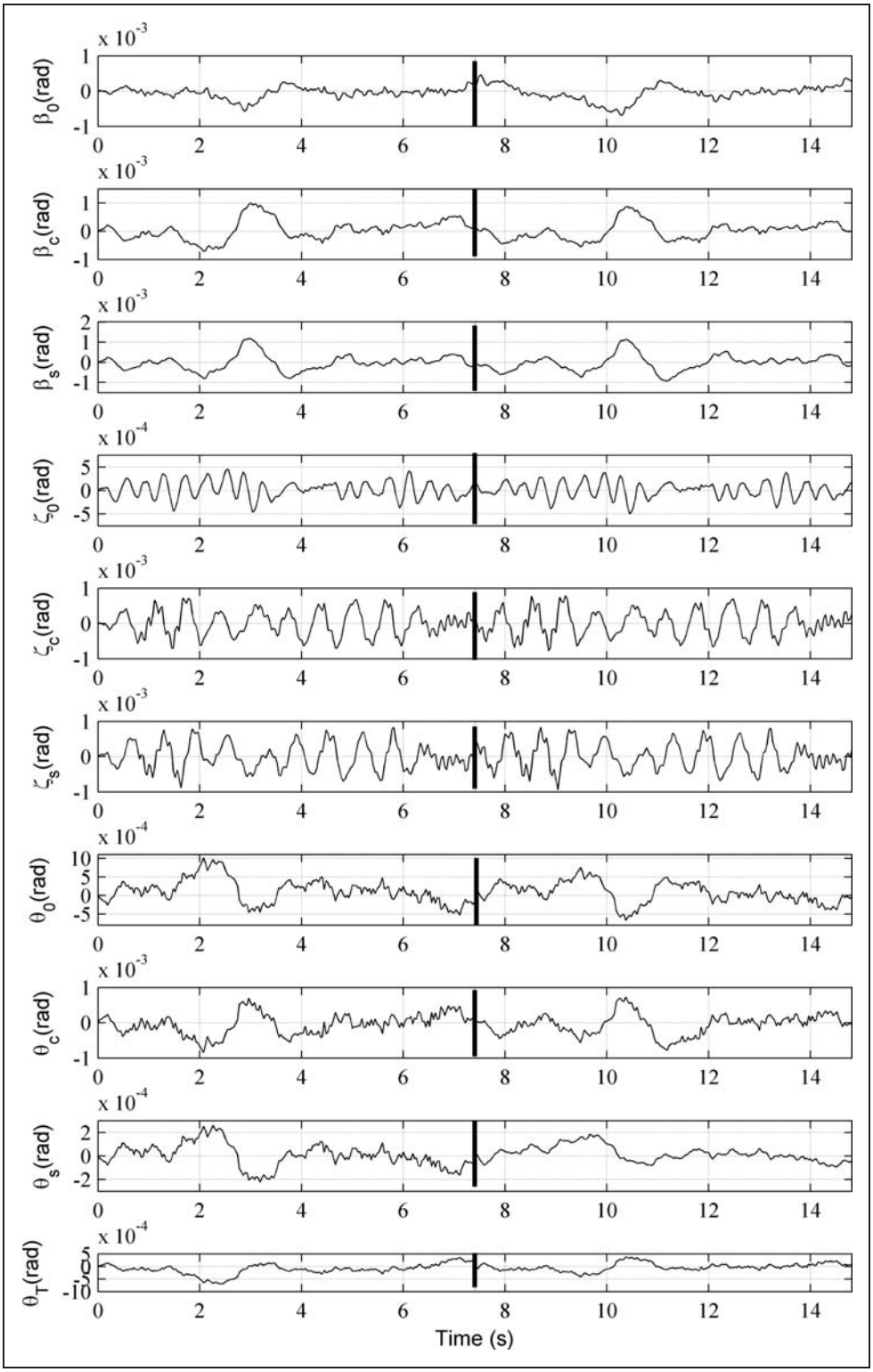

Figure 12. First IVC with first sensor failure (some blade states and all controls).

speed is $V_A = 80$ kts. These controllers are also robustly stable wrt uncertainty in helicopter inertial parameters. An important observation is that there is no correlation between the length of the stability interval, L, and the magnitudes of output or input constraints.

When sensor failure is considered, several important results are obtained. First, control design algorithms converge slower than when sensor failure does not occur. Second, for small number of failed sensors, the CL stability robustness wrt variations in V_A and helicopter inertial properties are very similar to the ones without sensor failure. Third, the control energy with sensor failure is higher than the control energy when sensor failure does not occur, which is a

reflection of the fact that controllers have to work harder to achieve specified variance constraints using less information from sensors. Fourth, when large sensor failures are considered, there are limitations in control design due to detectability issues related to the heading angle sensor. Moreover, constraints may not be satisfied (for OVC) and control energy consumption and robustness properties may be negatively impacted (for IVC).

Finally, adaptive switching of controllers in response to some sensor failures is investigated, showing that the switching idea can be used to mitigate sensor failure. The CL performance can be made qualitatively and quantitatively similar before and after sensor failure occurs if the controllers are switched to use the correct set of available sensors.

Funding

The corresponding author would like to express his gratitude to Republic of Turkey, Ministry of National Education for their financial support for his research. UTRC's partial technical support is also gratefully acknowledged.

References

1. Fusato D and Celi R. Multidisciplinary design optimization for helicopter aeromechanics and handling qualities. *J Aircr* 2006; 43(1): 241–252.
2. Fusato D, Guglieri G and Celi R. Flight dynamics of an articulated rotor helicopter with an external slung load. *J Am Helicopter Soc* 2001; 46(1): 3–14.
3. Sahasrabudhe V, Tischler M, Cheng R, et al. Balancing CH-53 K handling qualities and stability margin requirements in the presence of heavy external loads. In: *American helicopter society 63rd forum*, Virginia Beach, V, 1–3 May 2007.
4. Apkarian P, Champetier C and Magni JF. Design of a helicopter output feedback control law using modal and structured-robustness techniques. *Int J Control* 1989; 50(4): 1195–1215.
5. Altug E, Ostrowski JP and Mahony R. Control of a quadrotor helicopter using visual feedback. In: *Proceedings of the IEEE international conference on robotics and automation*, Washington, DC, USA, 11–15 May 2002.
6. Ivler CM, Tischler MB and Powell JD. Cable angle feedback control systems to improve handling qualities for helicopters with slung loads. In: *Proceedings of the AIAA guidance, navigation, and control conference*, Portland, OR, 8–11 August 2011.
7. Huang CY, Celi R and Shih IC. Reconfigurable flight control systems for a tandem rotor helicopter. *J Am Helicopter Soc* 1999; 44(1): 50–62.
8. Jiang Z, Han J, Wang Y, et al. Enhanced LQR control for unmanned helicopter in hover. In: *1st International symposium on systems and control in aerospace and astronautics*, Harbin, China, 19–21 January 2006.
9. Zhang WM. Hovering control and simulation of a tandem helicopter using LQR approach. *Microcomput Inf* 2010; 25: 172–174.
10. Bo LY, Zhu LW and Qi S. Improved LQG control for small unmanned helicopter based on active model in uncertain environment. In: *International conference on electronics, communications and control (ICECC)*, Ningbo, China, 9–11 September 2011.
11. Luo CC, Liu RF and Chang YH. Helicopter H∞ control design with robust flying quality. *Aerosp Sci Technol* 2003; 7: 159–169.
12. Kureemun R, Walker DJ, Manimala B, et al. Helicopter flight control law design using H∞ techniques. In: *Proceedings of the 44th IEEE conference on decision and control, and the European control conference 2005*, Seville, Spain, 12–15 December 2005.
13. Xie R, Wang X and Li Y. H∞ state feedback control for the stabilization of the three Euler angles of helicopter based on LMI. In: *International conference on intelligent computation technology and automation*, Hunan, China, 20–22 October 2008.
14. Bogdanov AA and Wan EA. Model predictive neural control of a high-fidelity helicopter model. In: *AIAA guidance navigation and control conference*, Montreal, QC, Canada, 6–9 August 2001.
15. Bottasso CL and Riviello L. Rotor trim by a neural model-predictive auto-pilot. In: *Proceedings of the 32nd European rotorcraft forum*, Florence, Italy, 13–15 September 2005.
16. Dalamagkidis K, Valavanis KP and Piegl LA. Nonlinear model predictive control with neural network optimization for autonomous autorotation of small unmanned helicopters. *IEEE Trans Control Syst Technol* 2010; 19(4): 1–14.
17. Oktay T. *Constrained control of complex helicopter models*. PhD Dissertation, Virginia Tech, Blacksburg, VA, 2012.
18. Oktay T and Sultan C. Integrated manuvering helicopter model and controller design. In: *AIAA guidance navigation and control conference*, Minneapolis, MN, 13–16 August 2012.
19. Oktay T and Sultan C. Model predictive control of manuvering helicopters and controller design. In: *AIAA guidance navigation and control conference*, Minneapolis, MN, 13–16 August 2012.
20. Skelton RE. *Dynamic systems control: linear systems analysis and synthesis*. New York: John Wiley & Sons, 1987, Chapter 8.
21. Skelton RE, Iwasaki T and Grigoriadis KM. *A unified algebraic approach to linear control design*. London: Taylor & Francis, 1998, Chapter 4.
22. Oktay T and Sultan C. Variance constrained control of maneuvering helicopters. In: *American helicopter society 68th forum*, Forth Worth, TX, USA, 1–3 May 2012.
23. Skelton RE and Lorenzo MD. Space structure control design by variance assignment. *J Guid Control Dyn* 1985; 8(4): 454–462.
24. Hsieh C, Skelton RE and Damra FM. Minimum energy controllers with inequality constraints on output variances. *Optim Control Appl Meth* 1989; 10(4): 347–366.
25. Zhu G and Skelton RE. Mixed L_2 and L_∞ problems by weight selection in quadratic optimal control. *Int J Quadratic Optim Control* 1991; 63(5): 1161–1176.
26. Zhu G, Rotea MA and Skelton RE. A convergent algorithm for the output covariance constraint control problem. *SIAM J Control Optim* 1997; 35(1): 341–361.

27. Skelton RE and Sultan C. Controllable tensegrity, a new class of smart structures. In: *SPIE international symposium on smart structures and materials*, San Diego, CA, 2–6 March 1997.
28. Sultan C and Skelton RE. Integrated design of controllable tensegrity structures. In: *Proceedings of the 1997 ASME international mechanical engineering congress and exposition*, Dallas, TX, 16–21 November 1997.
29. Tischler MB. *Advances in aircraft flight control*. London: Taylor & Francis, 1996, Chapter 4.
30. Heredia G and Ollero A. Sensor fault detection in small autonomous helicopters using observer/Kalman filter identification. In: *IEEE international conference on mechatronics*, Malaga, Spain, 14–17 April 2009.
31. Amato F, Cosentino C and Mattei M. A direct/functional redundancy scheme for fault detection and isolation on an aircraft. *Aerosp Sci Technol* 2006; 10(4): 338–345.
32. Sagoo GK, Gururajan S, Seanor B, et al. Evaluation of a fault tolerant scheme in a six-degree-of-freedom motion flight simulator. *J Aerosp Comput Inf Commun* 2010; 7(2): 47–67.
33. Waschburger R, Paiva HM, Silva JJR, et al. Fault detection in a laboratory helicopter employing a wavelet-based analytical redundancy approach. In: *Conference on control and fault tolerant systems*, Nice, France, 6–8 October 2010.
34. Xiao B and Hu Q. Fault-tolerant attitude control for flexible spacecraft without angular velocity magnitude measurement. *J Guid Control Dyn* 2011; 34(5): 1556–1560.
35. Chen RTN and Jeske JA. Kinematic properties of the helicopter in coordinated turns. NASA technical paper 1773, NASA, April 1981.
36. Celi R. Hingeless rotor dynamics in coordinated turns. *J Am Helicopter Soc* 1991; 36(4): 39–47.
37. Guglieri G and Celi R. On some aspects of helicopter flight dynamics in steady turns. *J Guid Control Dyn* 1998; 21(3): 383–390.
38. Prouty RW. *Helicopter performance, stability and control*. Malabar, FL: Robert E. Kreiger Publishing Co., 2005, pp.340–346.
39. Leishman JG. *Principles of helicopter aerodynamics*. Cambridge: Cambridge University Press, 2006, pp.263–265.
40. Padfield GD. *Helicopter flight dynamics*, AIAA Education Series. Washington DC, John Wiley & Sons, 2007, pp.265, 266, 293, 294.

Appendix

Notation

E_∞	expected value operator
p, q, r	angular velocities of helicopter in aircraft frame, (rad/s)
R_{turn}	turn radius, (m)
u, v, w	linear velocities of helicopter in aircraft frame, (m/s)
V_A	flight speed of helicopter, (kts)
x_A, y_A, z_A	aircraft frame unit vectors
$\beta_0, \beta_c, \beta_s$	collective and two cyclic blade flapping angles, (rad)
γ_{FP}	flight path angle, (rad)
$\zeta_0, \zeta_c, \zeta_s$	collective and two cyclic blade lead–lagging angles, (rad)
θ_T	collective pitch angle of tail, (rad)
$\theta_0, \theta_c, \theta_s$	collective and two cyclic blade pitch angles, (rad)
ϕ_A, θ_A, ψ_A	Euler angles of helicopter (roll, pitch, and yaw), (rad)
ψ	blade azimuth angle, (rad)
$(\,)^{\mathrm{T}}$	transpose